Advances in Science and Technology Research Journal

Advances in Science and Technology Research Journal, 2025, 19(1), 333–348
https://doi.org/10.12913/22998624/194205
ISSN 2299-8624, License CC-BY 4.0

Received: 2024.08.19
Accepted: 2024.11.15
Published: 2024.12.01

Experimental and numerical study on the effectiveness of the barrier protecting explosive against electric initiation system

Pawel Żochowski[1*], Bogdan Krysinski[1], Jan Bagrowski[1], Jacek Borkowski[1]

[1] Military Institute of Armament Technology, ul. Wyszynskiego 7, 05-220 Zielonka, Poland
* Corresponding author's e-mail: zochowskip@witu.mil.pl

ABSTRACT

Improvised explosive devices are responsible for death and injury of thousands of people (both civilians and soldiers) annually. They are often produced by simple home-made modifications of the old artillery shells. One of the ways of preventing modification of currently used artillery shells intended to make it more difficult to use as IEDs was analyzed in the article. A special safety barrier placed between the fuse and the explosive in order to block the access to the explosive after unscrewing the fuse was proposed. The barrier was used also to protect explosive against detonation with commonly used electric initiation systems. Therefore the main aim of the analyses presented in the article was to determine a critical barrier thickness for which the acceptor has 50% probability of being detonated. The research included experimental gap-tests as well as numerical reproduction of the phenomenon in the Impetus AFEA software. Various types of electric initiation systems were analyzed differing with material of the body, type and amount of explosive used as well as the shape of the frontal part of the detonator (flat or with hemispherical cavity). Critical barrier thicknesses were determined for individual variants of donor-gap-acceptor systems. Numerical model of the phenomenon was defined and validated against experimental data. Small differences between the experimental and numerical results allow to use the model to initial evaluation of the effectiveness of different barrier variants.

Keywords: gap-test, shock sensitiveness of explosives, improvised explosive devices, numerical simulations.

INTRODUCTION

Improvised explosive devices (IEDs) constitute one of the greatest threat to civilians and soldiers in modern asymmetric conflicts in the world [1]. Explosive devices may be considered as improvised when any of their structural components was modified from its original function. IEDs are responsible for death and injury of thousands of people annually [2]. Such a widespread use of IEDs results from their specific features – they are relatively cheap, easy to assemble, easy to use and highly effective at the same time. IEDs can be produced by modifications of conventional weapons (mines, artillery shells etc.). IEDs can also be manufactured by home methods by using ammunition-derived explosives, produced from commercially available chemicals, fertilizers with additional elements used to increase the amount of debris driven by the explosion: metal balls, nails, glass shards, etc. Various types of IEDs can be used depending on the intended target..

Relatively easy access of shells in the area of military conflict, low costs and high effectiveness of IEDs make them an ideal weapon of guerrilla forces, terrorist organizations, criminals, etc. Over the last decade IEDs constituted 42% of all recorded injurious explosive attacks. Nearly half of the people (48%) killed or injured by explosive weapons globally were harmed by IEDs [1]. Although 80% of those harmed were civilians, recent military operations in Iraq and Afghanistan showed that Improvised Explosive Devices (IED) are dangerous and lethal on the battlefield too [3]. For example, 48.7% of total military deaths (5,413) of US soldiers between September, 2011 and October 2020 were attributed to IEDs, mainly roadside bombs (73%), suicide bombs (16%), and car bombs (11%). At the same time 43% of total UK service personnel killed (634) were attributed to IEDs (32% in Iraq, 48 in Afghanistan) [1]. The continuously rising threat of the IED enforced the European Defense Agency (EDA) to start Counter-IED program in 2007. The international doctrine Countering IEDs consists of 6 key operational areas: Detect, Mitigate, Neutralize, Exploit, Predict, Prevent.

One of the ways of preventing modification of currently used artillery shells intended to make it more difficult to use as IEDs was analyzed in the article. In most of the currently used high-explosive shells, after unscrewing a fuse there is a direct access to the explosive material.

The explosive can be then easily extracted from the shell or a pocket in the explosive can be made in which an electric fuse may be placed and connected with a source of electrical impulse (Fig. 1) creating in this way a simple IED (Fig. 2).

In view of the above, it is advisable to prevent or to hinder the access to the explosive in the shell without reducing its original combat capabilities. Therefore a special safety barrier placed between the fuse and the explosive to block the access to the explosive after unscrewing the fuse was proposed (Fig. 3). The barrier is used also to protect explosive against detonation with commonly used electric initiation systems.

The idea of using a barrier inside an explosive shell is protected by patent in Polish Patent Office [5]. The optimal barrier should be non-removable and resistant to a destruction with available cutting tools or reagents. At the same time it should provide proper functioning of the shell. The barrier should not disturb the initiation process of the explosive with the use of original fuse. Therefore it is crucial to determine the suitable thickness of

Figure 2. IEDs made of explosive shells and an antipersonnel mine [4]

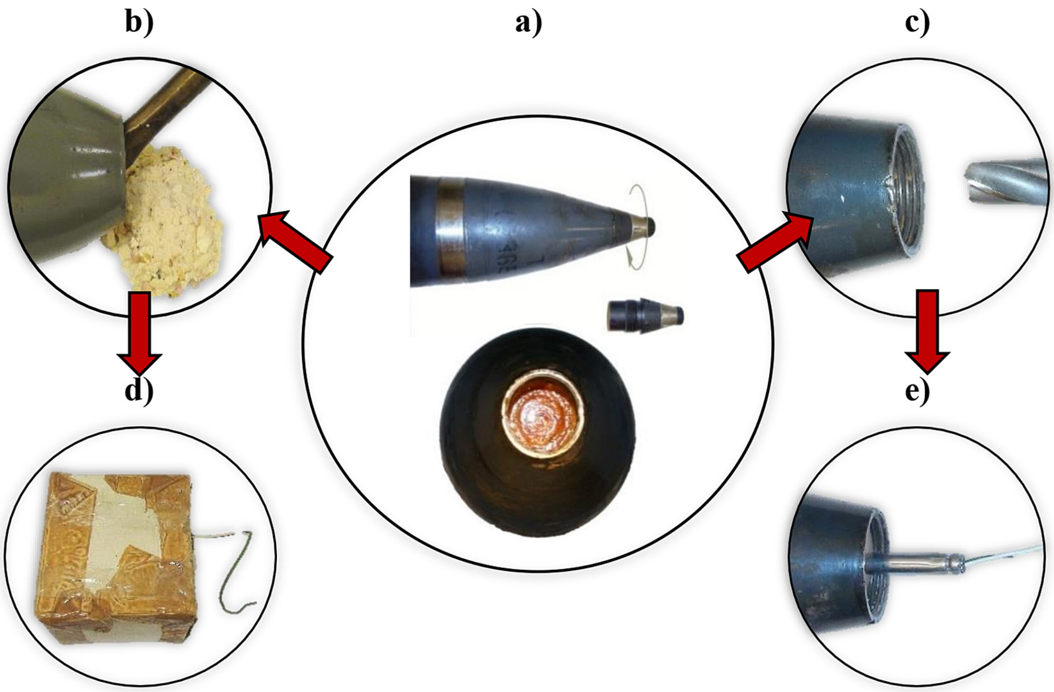

Figure 1. Examples of possible ways of creating IEDs from explosive shells: (a) unscrewing the fuse and direct access to the explosive, (b) extraction of the explosive, (c) drilling the nest for external detonator, (d) using of the explosive in improvised devices, (e) using of external detonator in artillery shell

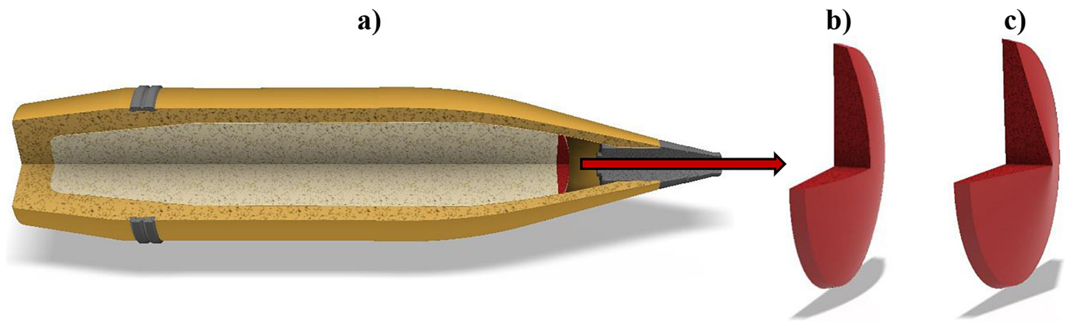

Figure 3. Examples of barrier shapes and their position in an explosive shell: (a) explosive shell, (b) (c) barrier variants

the barrier, which on the one hand should be thin enough to allow the original fuse of the shell to initiate the explosive, on the other hand it should be thick enough to prevent detonation by the external initiation systems.

Shock sensitivity of the explosive is the main factor that influence the required thickness of such barrier. It can be can be quantified by the critical shock wave initiation pressure parameter. Different experimental and theoretical procedures are used to measure the initiation capacity of the explosives [6–13]. The paper [11] investigates the characteristics of shock waves in soil due to the explosion of a cylindrical explosive charge. The main purpose of the analysis was to study the dependence of the peak stress attenuation during the shock wave propagation on the full locking parameter. A new modeling method of shock wave overpressure under free-field air explosion was proposed in the work [10] expressed as a product of the three factor functions of peak, attenuation and oscillation. In the works [12, 13] the authors performed shock sensitivity experiments on TATB/HMX-based PBX explosives with various particle size and porosity. The results indicated that together with the decrease of the particle size, the ignition of the explosive become more difficult but the detonation grows more rapidly when the explosive is ignited. Shock wave sensitivity of eleven explosives were analyzed by the authors in the work [14] with the use of the gap test with aluminum barriers. The peak shock pressure and the shock sensitivity curves were determined for the PBXN-109 explosive with the use of combined experimental and numerical study in the work [15]. The shock induced detonation sensitivity of an explosive was analyzed in the work [16] using the shock Hugoniots of the condensed material and the detonation products.

Shock sensitivity of the explosive is most frequently assessed with the use of various modifications of classic gap tests [17–20]. The test usually consists of four components: a donor charge, a gap/attentuator, an acceptor charge, and a witness plate. The donor is usually detonated by an electrical initiation system. Detonation generates the shock wave that travels through the donor and is attenuated through the gap. The pressure attenuated by the gap determines whether the transmitted shock wave will trigger an acceptor or not. If the acceptor is detonated, a hole is created at the witness plate. The thickness of the gap thickness is adjusted, in order to determine its critical value. A critical gap thickness for which the acceptor has 50% probability of being detonated marks the shock sensitivity of the acceptor [21–24]. The critical gap/barrier thickness determined during the gap test can be used to define the shock wave initiation capacity of explosives as well as to compare their detonation sensitivity. [13, 15, 16, 25–27]

Beside the classic experimental tests, recently (thanks to the rapid growth of the computational power of modern computers) numerical methods are often used to simulate the gap tests. It allows to reduce the costs of analyses as well as to gather more information about the entire phenomenon, e.g. pressure, density or velocity distribution at different times. Various numerical methods are used in analysis of explosive shock sensitiveness. In the work [19] finite difference technique was used to simulate gap-test of Composition B. Two-dimensional Eulerian hydrodynamic code was used in the work [20] to simulate sympathetic detonation. The authors found that critical gap length and the charge weight approximately have a linear relationship with a logarithmic scale. Ls-Dyna and ALE multi-material formulation were used in the work [28] to simulate a blunt brass projectile impacting COMP-B charges without and with metal cover plates. The minimal velocity of the projectile required to detonation of the explosive was evaluated and compared with experimental data. In the works [29, 30] shock initiation experiments on the explosives Composition B and C-4 were simulated with the use of Ignition and Growth reactive flow model implemented in LS-Dyna. Typical gap tests test was simulated in work [25] to obtain the shock wave critical initiation pressure of RDX-based mixed explosive, HMX-based mixed explosive, and RDX/AP/Al-based propellant mixed explosive. The results indicated that the shock wave sensitivity and initiation capacity of RDX-based and HMX-based mixed explosives are higher than TNT. In the work [31] the authors experimentally analyzed desensitization of high explosive charges in water gap test and then successfully simulated the phenomenon using the Lee–Tarver material model. On the basis of the results the conclusion was drawn that that precursor waves in gap test assemblies can affect the detonation propagation distance. Numerical model of the small scale gap test was proposed in the work [8]. Simulation of the small scale gap test were carried out in the LS-Dyna software. On the basis of the calculations results the detonation characteristics were determined for the mixed explosives. On the basis of the literature review it can be concluded that numerical simulations constitute a helpful tool supporting experimental analyses of explosives shock sensitivity and gap-tests. The main aim of the work presented in the article was to analyze the effectiveness of the proposed solution intended to prevent modification of currently used artillery shells in a way allowing their use as IEDs. The research included experimental gap-tests as well as numerical reproduction of the phenomenon in the Impetus AFEA software. Analyses were carried out to determine a critical thickness of the special safety barrier placed between the fuse and the explosive in artillery shells in order to block the access to the explosive after unscrewing the fuse.

MATERIALS AND METHODS

Experimental methodology

The experimental tests have been performed at Military Institute of Armament Technology (MIAT) proving ground, in Poland. Simple modification of the conventional gap-test procedure was used. Figure 4 presents a gap test assembly.

In the presented assembly electric detonator constituted a donor charge. A gap/barrier was made of high-strength steel plate with hardness of 63–65 HRC and thickness varied from 2 to 3.5 mm. A cylinder made of TNT was an acceptor. After assembling components were placed at the steel plate of the 6 mm thickness. The witness plate was placed at the steel tube. Eight types of donors were prepared for the tests (Fig. 5). They had body made of different materials – aluminum

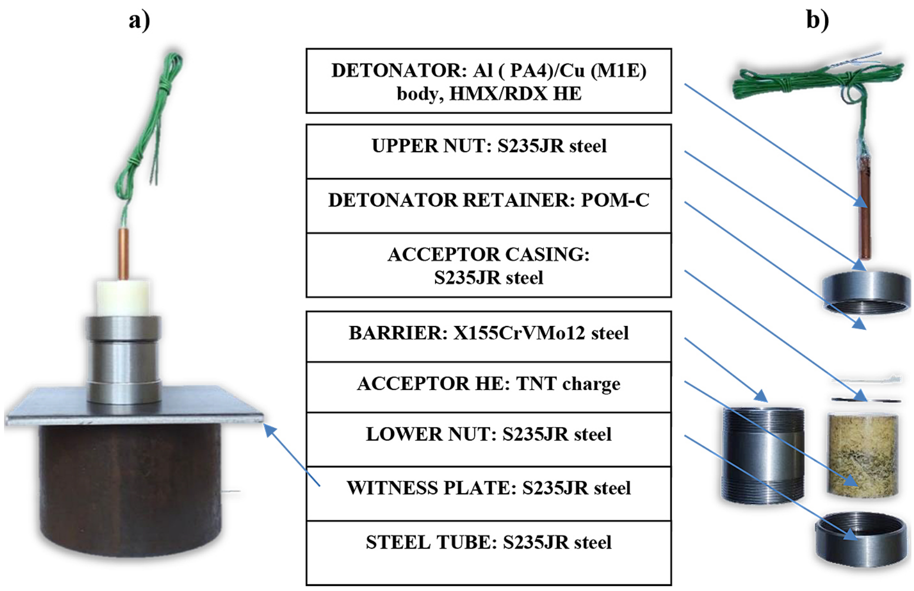

Figure 4. Experimental gap-test: (a) assembled, (b) disassembled

alloy and copper, different shapes of frontal part of the detonators – flat or with spherical cavity, and they were filled with different explosives: HMX or RDX.

Materials

HMX and RDX – donor explosives

HMX, or octahydro-1,3,5,7-tetranitro-1,3,5,7-tetrazocine, is a powerful high explosive with excellent stability and performance characteristics. It belongs to the nitramine class of explosives and is widely used in military and industrial applications. HMX is known for its high density, high detonation velocity, and low sensitivity to impact and friction, making it a valuable component in various munitions and propellants.

- molecular weight – approximately 296.15 g/mol;
- density – ranging from 1.91 to 1.97 g/cm^3;
- melting point – around 276–277 °C.

HMX is a key ingredient in several high-performance explosive formulations. The synthesis of HMX involves the nitration of hexamethylenetetramine. RDX, or cyclotrimethylenetrinitramine is a powerful high explosive from the category of nitramines. RDX is widely used in military and industrial applications due to its high stability, insensitivity to shock and friction, and excellent explosive performance.

- molecular weight – approximately 222.10 g/mol
- density – ranging from 1.80 to 1.82 g/cm^3.
- melting point – around 204–205 °C.

RDX is a key component in various explosive formulations. The synthesis of RDX typically involves the nitration of hexamine (hexamethylenetetramine) in the presence of concentrated nitric acid and acetic anhydride. In the conducted research, ERG detonators were used, in which RDX or HMX charges were pressed to a density ranging from 1.4 to 1.42 g/cm^3

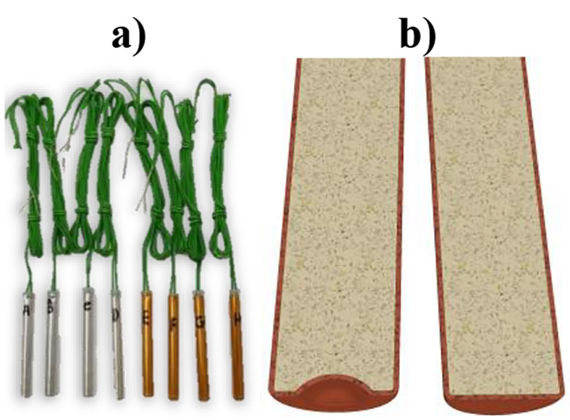

Figure 5. Analyzed detonator variants: (a) made of aluminum alloy and copper; (b) with and without a cavity in the frontal part

TNT – acceptor explosive

Trinitrotoluene, commonly known as TNT, is a chemical compound with the molecular formula C7H5N3O6. It is a pale yellow, crystalline solid that is renowned for its explosive properties. TNT is produced by the nitration of toluene and is widely used as a high explosive in various applications, including military, industrial, and mining. It is relatively stable under normal conditions but can be detonated by a shock or heat. TNT has been a crucial component in the development of explosives and is employed in the manufacturing of munitions, dynamite, and other explosive devices. Its controlled and predictable properties make it a valuable explosive for a range of applications.

In this research, TNT charges pressed at a pressure of 300 MPa were used as acceptors. Examples of these charges, their dimensions and masses, and the determined density values are given in Table 1.

Copper and Al – ERG detonator body

The tests used ERG fuzes with two versions of aluminum or copper shells. The physico-chemical properties of these materials are given in Tables 2 and 3.

POM-C – donor retainer

The donor retained in the study was made of polyacetal copolymer POM-C (TECAFORM AH) inert material. POM-C is a high-performance engineering plastic characterized by its excellent mechanical and chemical properties. POM-C is a thermoplastic material, which means it can be repeatedly melted and solidified without significant degradation of its properties. POM-C exhibits high tensile strength, stiffness, and impact resistance. This makes it suitable for applications where mechanical performance is crucial. POM-C has low friction properties, making it an excellent material for applications where sliding or rotating parts are involved. It also has good wear resistance, contributing to its durability. POM-C has good dimensional stability, maintaining its shape and size under different temperature

Table 1. Examples of TNT charges

Nb.	Nb. charge	Ø [mm]	h [mm]	m [g]	V [cm³]	rh0 [g/cm³]
1	14 / 32	42.17	44.9	100.43	62.711	1.601
2	15 / 33	42.15	44.74	100.36	62.428	1.608
3	16 / 34	42.17	44.93	100.36	62.753	1.599
4	17 / 35	42.19	44.78	100.31	62.603	1.602
5	18 / 36	42.16	44.93	100.38	62.723	1.600
6	19 / 37	42.15	44.9	100.41	62.651	1.603
7	20 / 38	42.16	44.98	100.36	62.793	1.598
8	21 / 39	42.18	44.82	100.42	62.629	1.603
9	22 / 40	42.14	44.89	100.22	62.608	1.601
10	23 / 41	42.18	44.79	100.32	62.587	1.603
11	24 / 42	42.19	45.01	100.3	62.924	1.594
12	25 / 43	42.23	45.09	100.39	63.156	1.590
					Medium density	1.600
					Standard deviation	0.005

Table 2. Chemical composition and mechanical properties of the copper material

Cu	Bi	O_2	Pb	Density, [g/cm³]	Young modulus, [GPa]
99.9 min.	0.0005 max	0.04 max	0.005 max	8.9	127

Table 3. Chemical composition (%) and mechanical properties of the PA4 / 6082 aluminum alloy

Si	Fe	Cu	Mn	Mg	Cr	Zn	Ni	Zr	Ti
0.7	0.45	0.08	0.4	0.6	0.23	0.18	-	-	0.08
1.3	0.55	0.12	1	1.2	0.27	0.22	-	-	0.12
Hardness:	Density [g/cm³]								

and humidity conditions. POM-C is known for its ease of machinability. It can be machined into precision components with tight tolerances. Applications of POM-C include gears, bearings, bushings, precision mechanical components, automotive parts, and various industrial components where a combination of high strength, low friction, and durability is required. Structural formula and basic properties of POM-C were shown in Table 4. The mechanical properties of POM-C have been already determined by the team of the authors in work [32] where quasi-static tension and compression tests were carried out in order to collect data (force-displacement curves) allowing subsequent definition and validation of numerical models of the POM-C material.

NC10 / 1.2201 steel - barrier

The tests used barriers made of NC10 steel, hardened to a hardness of 60 to 63 HRC. The composition and physical properties of this steel are given in Table 5.

S235JR steel – structural components

S235 is a designation in the EN 10025 standard for a structural steel grade with the minimum

Table 4. Mechanical properties of the POM-C material [48]

Density [g/cm³]	Yield strength [MPa]	Tensile strength [MPa]	Young modulus [GPa]	Shear Modulus, [GPa]	Hardness (Rockwell M)	Elongation at break, %
1.41	67	67	2.8	1.1	88	32

Table 5. Chemical composition (%) and mechanical properties of the NC10 / 1.2201 steel

C	Si	Mn	Cr	Mo	Ni	Cu	W	S max	P max
1.5	0.15	0.15	11	Max	Max	Max	-	-	-
1.8	0.4	0.45	13	0.04	0.1	0.13	-	0.03	0.03
Hardness in a softened state, HB			Hardness in heat-treated condition, HRC						
255			60						

yield strength of 235 MPa. S235 steel is commonly used in construction and structural engineering applications due to its good combination of strength and weldability. The alloy composition and basic physical properties of this material are presented in Table 6.

EXPERIMENTAL RESULTS AND ANALYSIS

Evaluation of the effectiveness of detonation of the TNT charge through the steel plate barrier was carried out on the basis of traces left on the steel plate, the so-called witness. If the donor (ERG electric detonator) initiated the acceptor (TNT cylinder) into detonation, a hole with a diameter of several cm was formed in the steel plate (Fig. 6a). In the absence of successful initiation of the TNT cube by the donor, the plate bore little or no signs of deformation (Fig. 6b). The partition, on the other hand, was damaged depending on its thickness and the type of igniter used (Fig. 6c).

The results obtained from the tests of TNT initiation through the barrier as a function of the type of detonator (fuse) and the thickness of the barrier are shown in Table 7.

It was assumed that the absence of initiation to detonation of a TNT charge in three tests for one plate thickness by a given version of the ERG detonator, is a positive result of the test. It proves that the required effectiveness of blocking the effects of the ERG detonator on the TNT charge is met by the barrier.

On the basis of the tests, it should be noted that in the case of the use of a detonator with a flat frontal surface, no initiation of the TNT charge was observed even for the thinnest 1.5 mm thick barrier used during the tests. In the case of a copper detonator with a shaped (with a cavity) front part, the limiting thickness of the barrier preventing detonation is in the range of 2.0–2.5 mm for 1.24 g RDX and 2.5–3.0 mm for 1.18 g HMX.

For an aluminum detonator with a shaped face section, the limiting thickness of the barrier preventing detonation is in the range of 2.5–3 mm for 1.18 g HMX and 3–3.5 mm for 1.06 g RDX. Obtaining initiation for a detonator with RDX through a thicker barrier than for a detonator with HMX may be due to several reasons. One of them is the difference in the accuracy of making the cumulative cavity in the detonator casing. In addition, there may have been a slight difference in the size of the explosive weight.

Table 6. Chemical composition (%) and mechanical properties of the S235JR(10025-2) steel

C	Mn	P	S	N	Cu
≤ 0.17	≤ 1.40	≤ 0.035	≤ 0.035	≤ 0.12	≤ 0.55
Minimum yield strength Re, (MPa)			Strength limit, Rm (MPa)		

a) b) c)

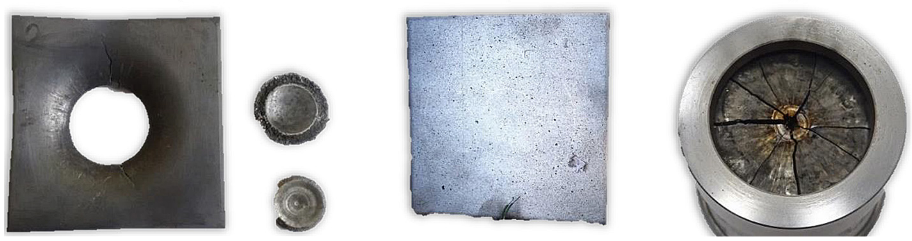

Figure 6. Deformations of witness plate: a – in case of detonation of TNT, b – in case of no detonation of TNT

Table 7. Results of experimental tests

Type of the donor				Thickness of the barier, [mm]			
Body material	Explosive material	Shape of frontal part	1.5	2.0	2.5	3.0	3.5
Al	RDX 1.06 g	Flat	-	- - -			
Al	RDX 1.06 g	Cavity		+ +	+	- +	- - -
Al	HMX 1.18 g	Flat		- - -			
Al	HMX 1.18 g	Cavity			+	- - -	
Cu	RDX 1.24 g	Flat	-	- - -			
Cu	RDX 1.24 g	Cavity	+	+ +	- - -	-	
Cu	HMX 1.18 g	Flat		- - -			
Cu	HMX 1.18 g	Cavity			- + -	- - -	

Note: + detonation, - no detonation.

The detonators for the tests were not made using a laboratory method and, therefore, the tolerance range of their manufacturing was adopted according to the technical documentation of such a product. Therefore, such a result should be considered accidental.

The results of the study showed that detonators with a shaped face part initiate TNT charges through significantly thicker (at least three times) steel barriers compared to the action of detonators with a flat face. This is due to the fact that the spherical indentation of the detonator's face section allows the energy of the detonation products to be concentrated along the axis of symmetry and the formation of a kind of shaped charge jet, while in the flat case there is a divergent shock wave loading. In both cases, the ability to initiate the detonation of a TNT charge is a function of the thickness of the steel barrier, which reduces both the velocity of the jet elements and the intensity of the shock wave, which constitute the effective load capable of causing detonation of the charge.

The conducted research should be taken as the first step in the area of determining the dimensional and material characteristics of the barriers blocking access to explosives deployed in munitions, through which it will not be possible to effectively excite them with an ERG-type detonator.

The results of the research make it possible to take measures to introduce such a barrier into products containing explosive material. This will significantly reduce the possibility of its acquisition for terrorist purposes or the use of such devices for adaptation to an improvised explosive device (IED).

NUMERICAL SIMULATIONS

Modeling procedure

Numerical reproduction of the gap tests were carried out in the Impetus AFEA software [33]. A three-dimensional (3D) model with two symmetry planes was developed with a γSPH formulation [34]. The γSPH formulation allows simulating high strains of materials without the problems related to the mesh distortions. The γSPH™ is a modernized version of the classic smooth particle hydrodynamic method (SPH), with a strong emphasis on eliminating characteristic drawbacks related primarily to instability phenomena during stretching and perturbed and distorted pressure fields. In addition, the γSPH™ solver makes full use of GPU technology for parallel calculations on single or multiple GPUs. By using the power of GPU for calculations, engineering problems consisting of tens of millions of particles can be solved in a very short time.

Numerical model of the analyzed phenomenon was shown in Figure 7. All components of simulations were described by γSPH particles. Filling the components with particles requires only the creation of surface meshes determining the volume of the components. It is required that the surface meshes are made of triangular shell elements with normal vectors directed outside the defined volume. Then the algorithm is able to correctly fill the volume with particles according to the user-defined density (distance between neighboring particles). Discretization of the initial model (subsequently filled with γSPH particles) was performed using ALTAIR HyperMesh software. Numerical model of the gap-test consisted of 10 parts with the appropriate materials assigned.

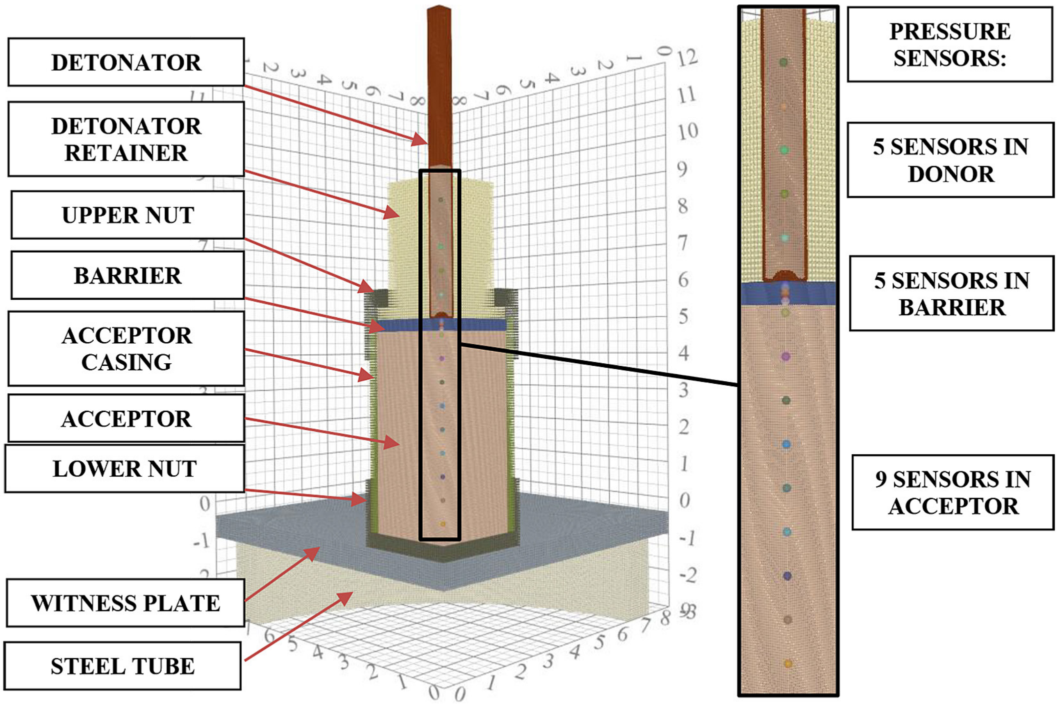

Figure 7. Numerical model of the analyzed phenomenon

Additionally, fixed sensors were defined along the axis, that had the ability to register the most important physical parameters of the analyzed phenomenon – in this case, measurements of the pressure present in both the explosives and the barrier were crucial. Finally all the components of simulation were discretized with 4 500 000 γSPH™ particles.

Constitutive equations

A few different material models available in Impetus AFEA software [35] were used in the simulations. Parameters of the material models were adopted from literature and ANSYS Autodyn [36] software material libraries. Three general types of materials were modeled in the work:

- Metals – steel, copper and aluminum alloys that were used in structural components (donor body and barrier);
- Explosives (RDX or HMX in donor and TNT in acceptor charges);
- POM-C plastic material.

Structural components

The material model proposed by Johnson and Cook (J-C) [37] was used to describe the behaviour of the metallic components in the analysed phenomenon It is defined with the following formula:

$$\sigma = (A + B\varepsilon^n)\left(1 + Cln\frac{\dot{\varepsilon}}{\dot{\varepsilon}_0}\right)\left[1 - \left(\frac{T-T_r}{T_m-T_r}\right)^m\right] \quad (1)$$

where: σ – Von Mises equivalent stress, *A* – quasi-static yield strength of the material at room temperature, *B* – strength constant, *n* – strength exponent, ε – equivalent plastic deformation, $\dot{\varepsilon}$ – plastic strain rate, $\dot{\varepsilon}_0$ – initial strain rate, *C* – strain rate sensitivity coefficient, *m* – temperature softening coefficient, T_m – melting temperature of the material, T_r – reference temperature (normal temperature), *T* – current temperature.

The JC material model was supplemented with the Cockcroft-Latham (CL) failure criterion. Ductile damage in CL damage model is described by the following equation:

$$D_d = \frac{1}{W_c}\int_0^{\varepsilon^p_{eff}} \max(0, \sigma_1)\, d\varepsilon^p_{eff} \quad (2)$$

where: σ_1 is the maximum principal stress. The complementing tensile damage is defined as:

$$D_t = \frac{1}{t_s}\int_0^t (\bar{\sigma}_1/\sigma_s)^{\alpha_s} dt \quad (3)$$

where: $\bar{\sigma}_1$ is defined as:

$$\bar{\sigma}_1 = \sigma_1^{dev} - (1 - \beta_s)p \quad (4)$$

where: $\sigma_1^{dev}\sigma_1^{dev}$ is the maximum deviatoric principal stress and p is the pressure.

With $\beta_s = 0$, $\bar{\sigma}_1$ equals the maximum principal stress. Tensile fracture/spalling term only contributes to the damage growth if $\bar{\sigma}_1 \geq \sigma_s \bar{\sigma}_1 \geq \sigma_s$. The material is assumed to fail when one of the damage parameters reaches 1 [35].

Gruneisen equation of state (EOS) which is usually used for describing materials in the high velocity impacts scenarios was used in the simulations. The EOS defines pressure for the materials that are compressed or expanded. The EOS includes the effects of internal Energy via the Gruneisen parameter. The Gruneisen equation of state with cubic shock-velocity as a function of particle velocity (vp) defines pressure for compressed materials as [35]]:

- for compressed materials:

$$P = \frac{\rho_0 C^2 \mu \left[1 + \left(1 - \frac{\gamma_0}{2}\right)\mu - \frac{a}{2}\mu^2\right]}{\left[1 - (S_1 - 1)\mu - S_2 \frac{\mu^2}{\mu + 1} - S_3 \frac{\mu^3}{(\mu + 1)^2}\right]} + (\gamma_0 + a\mu)E \tag{5}$$

- for expanded materials:

$$P = \rho_0 C^2 \mu + (\gamma_0 + a\mu)E \tag{6}$$

where: C – intercept of the *vs(vp)* curve (in velocity units), S_1, S_2 and S_3 – unitless coefficients of the slope of the *vs(vp)* curve, γ_0 – unitless Gruneisen gamma coefficient, α – unitless, first order volume correction to γ_0, $\mu = (\rho/\rho_0)$-1, E – specific internal energy.

Values of material parameters of the metallic components of the analyzed phenomenon were presented in Table 8.

Explosive and detonation products

The donor explosive was described with JC flow model and Jones-Wilkins-Lee equations of state (JWL). The Lee-Tarver (LT) reactive burn model was used to model the acceptor explosive response. The LT model is used whenever it is uncertain whether the HE will react, there is a finite time required for a shock wave to build up to detonation, and/or there is a finite thickness of the chemical reaction zone in a detonation wave [35, 38]. In the LT model the JWL equation of state defines the pressure in the unreacted explosive as [35]:

$$p_u = A_u \left(1 - \frac{\omega_u}{R_{1,u} V_u}\right) e^{-R_{1,u} V_u} + B_u \left(1 - \frac{\omega_u}{R_{2,u} V_u}\right) e^{-R_{2,u} V_u} + \omega_u e_u \tag{7}$$

where: A_u, B_u, R_1, R_2, ω_u are unreacted JWL constant V_u is the relative volume of the unreacted material and e_u is the specific internal energy of the unreacted material.

Another JWL equation of state defines the pressure in the reaction products as:

$$p_r = A_r \left(1 - \frac{\omega_r}{R_{1,r} V_r}\right) e^{-R_{1,r} V_r} + B_r \left(1 - \frac{\omega_r}{R_{2,r} V_r}\right) e^{-R_{2,r} V_r} + \omega_r e_r \tag{8}$$

There is assumed be a pressure equilibrium between the phases in a mixture of unburned and burned material $p \equiv p_u \equiv p_r$. This is achieved by adjusting the relative volumes of the phases while maintaining: As the chemical reaction converts unreacted explosive to reaction products, these JWL equations of state are used to calculate the mixture of unreacted explosive and reaction products defined by the fraction reacted F(F = 0 implies no reaction, F = 1 implies complete reaction). The temperatures and pressures are assumed to be equal ($T_u = T_r$, $p_u = p_r$) and the relative volumes of the phases equal:

$$V = (1 - F)V_u + FV_r \tag{9}$$

where: V is the relative volume of the mixture, i.e. the ratio of initial to current density:

$$V = \frac{\rho_0}{\rho} \tag{10}$$

The chemical reaction rate for conversion of unreacted explosive to reaction products consists of three physically realistic terms:

$$\frac{dF}{dt} = \frac{dF_1}{dt} + \frac{dF_2}{dt} + \frac{dF_3}{dt} \tag{11}$$

Table 8. Material parameters of the metallic components used in simulations

Parameter	RO, [g/cm³]	G, [GPA]	v	A, [MPa]	B, [MPa]	n	C	m	S1	γ	Source
OFHC copper	8.96	46	0.33	90	292	0.31	0.03	1.09	1.49	2.02	[36]
Al2024	2.7	28	0.31	352	440	0.42	0.01	1	1.33	2.0	[36]
S235jr steel	7.85	77	0.3	235	350	0.26	0.014	1	1.49	2.17	OWN
NC11LV steel	7.85	77	0.33	860	500	0.26	0.014	1	1.73	1.67	OWN

- an ignition term in which a small amount of explosive reacts soon after the shock wave compresses it

$$\frac{dF_1}{dt} = \begin{cases} I(1-F)^b(\frac{\rho_0}{\rho} - 1 - a)^x : F \le F_1 \\ 0 : F > F_1 \end{cases} \quad (12)$$

- a slow growth of reaction (hot spots) as this initial reaction spreads;

$$\frac{dF_2}{dt} = \begin{cases} G_1(1-F)^c F^d(\frac{p}{p_0})^y : F \le F_2 \\ 0 : F > F_2 \end{cases} \quad (13)$$

- a rapid completion of reaction at high pressure and temperature.

$$\frac{dF_3}{dt} = \begin{cases} 0 : F < F_3 \\ G_2(1-F)^e F^g(\frac{p}{p_0})^z : F \ge F_3 \end{cases} \quad (14)$$

where: I, b, a, x – constants in ignition term of reaction equation; G_1, c, d, y – constants in growth term of reaction equation; G_2, e, g, z – constant in completion term of reaction equation.

The parameters of the donor and acceptor explosives used in simulations were shown in Tables 9, 10. Due to the lack of verified material parameters for TNT they were adopted like for Comp-B explosive.

NUMERICAL SIMULATION RESULTS AND ANALYSIS

The main aim of the simulations was reproducing of the gap test experiments performed earlier and comparison of results obtained numerically and experimentally. In case of small differences between the results, the methodology based on numerical simulation could constitute an effective tool supporting experimental procedures of gap tests. Therefore numerical reproduction of the gap tests were carried out in the Impetus AFEA software [33]. Similar like in experiments the presence/absence of detonation in acceptor explosive was assessed. Due to the lack of some factors confirming the detonation, which are characteristic to experiments (visible light, heat, shockwaves, sound) in numerical simulations it was confirmed in different way. Firstly the most obvious deformation and damage of the simulation components were compared. The results of simulation of the gap tests for the detonators with aluminum body and semi-spherical cavity were shown in Figures 8–9. In case where no detonation was observed only the components of electrical fuse and its retainer were destroyed (Fig. 8). The barrier and the components below the barrier remained almost untouched.

In case of detonation the structural components of the testing stand were completely destroyed and a large perforation hole (radius of about 4 cm) was created in a witness plate (Fig. 9), similar like in experiments (Fig. 6a).

In the Figure 10 the comparison of pressure waves propagation for the mentioned two variants of barrier thickness (2.0 mm and 2.5 mm) were shown. Detonation was observed only in case of the thinner barrier.

Secondly the shock wave criterion for detonation was used based on the value of Chapman-Jouquet (C-J) pressure. The C-J pressure is the point where the Rayleigh line is tangent to the Hugoniot. At pressures below the C-J pressure, detonation, or deflagration, may also occur. Above the C-J pressure only detonation occurs. The value of C-J pressure for acceptor explosive- TNT was defined to 24 GPa. Therefore the pressure in the explosives was monitored during the analyses by

Table 9. Material parameters of the donor explosives – HMX and RDX

	RO, g/cm^3	D, km/s	PCJ, GPa	A, GPa	B, GPa	R1	R2	ω	EO, kJ/m^3	VO	SOURCE
RDX	1.72e	7.98	29.5	524	7.67	4.2	1.1	0.34	8500	1	[36]
HMX	1.891	9.1	42	778	7.07	4.2	1	0.3	10500	1	[36]

Table 10. Material parameters of the acceptor explosive – TNT

A_u	B_u	$R_{1,u}$	$R_{2,u}$	ω_u	A_r	B_r	$R_{1,r}$	$R_{2,r}$	ω_r	$e_{0,r}$	p_0	a	b
485	-0.039	11.3	1.13	0.8938	5.242	0.0767	4.2	1.1	0.5	0.085	1	0.0367	0.667
c	d	e	g	I	x	y	z	F_1	F_2	F_3	G_1	G_2	
0.667	0.333	0.222	1	40	7	2	3	0.022	0.7	0	140	1000	

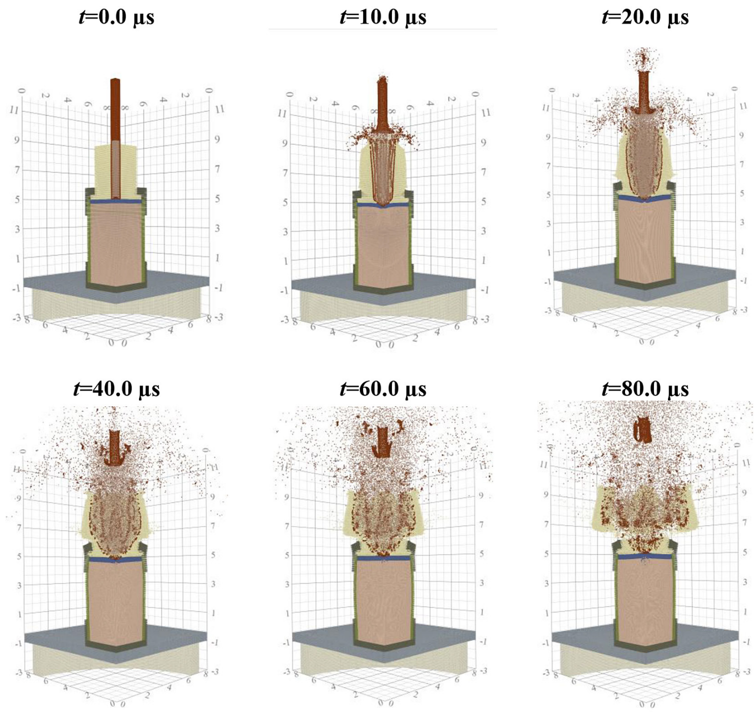

Figure 8. The course of the Gap-test simulation process and deformation of components for the "no detonation" case (2.5 mm thick barrier)

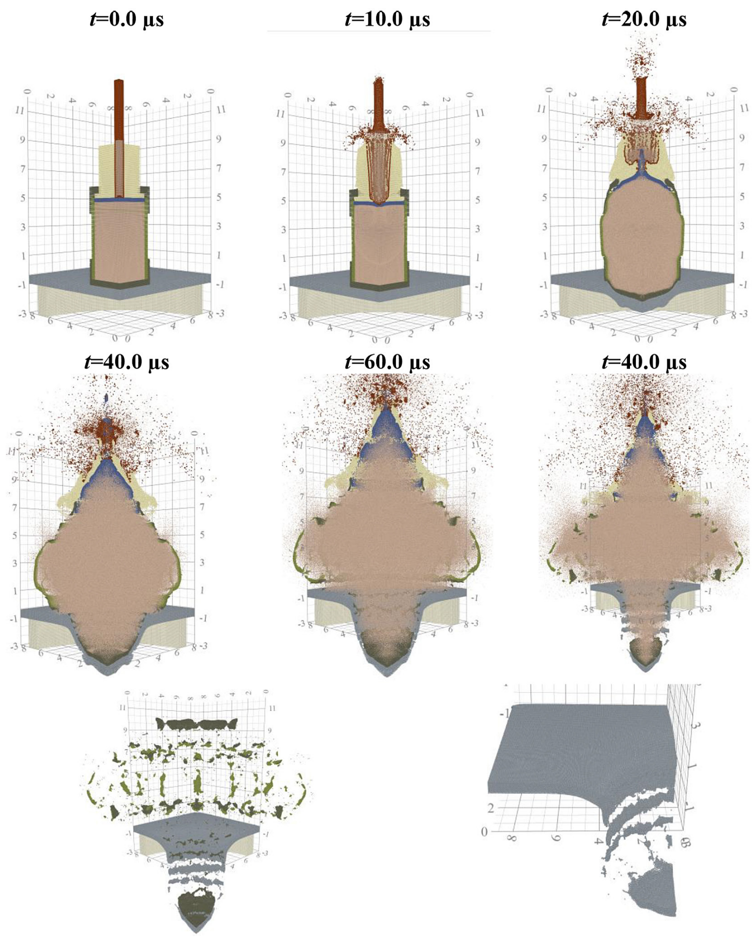

Figure 9. The course of the Gap-test simulation process and deformation of components for the detonation case (2-mm thick barrier)

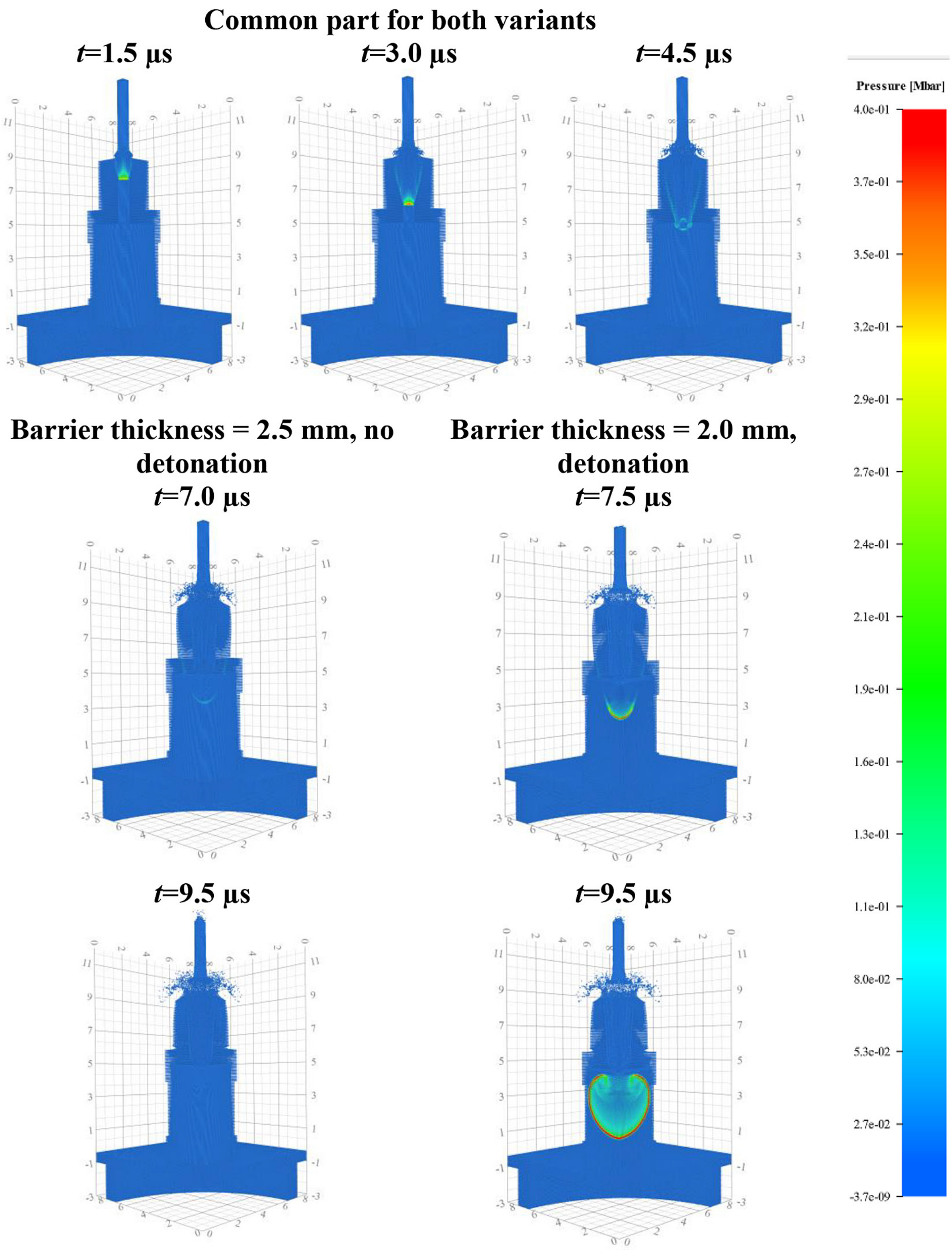

Figure 10. Fringe of the pressure history variable for the barrier of the 2.5 mm and 2.0 mm thickness

defining sensors located along the axis of symmetry. The initial location of the sensors was shown in Figure 6. The pressure plots recorded at the following tracers were shown in Figure 11 and 12 for the variants without and with detonation respectively. It is clearly visible that in case of detonation (Fig. 10) the maximum pressure increased nearly linearly with distance into the TNT, i.e. moving from the bottom surface of the barrier (Sensor 11) to more distant from the barrier (sensor 19) and were close to the C-J pressure. Such characteristic peaks of pressure were not observed in case of thicker barrier and no detonation case (Figure 11).

According to described methodology of simulations analyses were carried out for all the variants of detonators that were used in experiments and high correlation was obtained. Built and verified against experimental data, the numerical model of the analyzed phenomenon can provide effective support for experimental methods

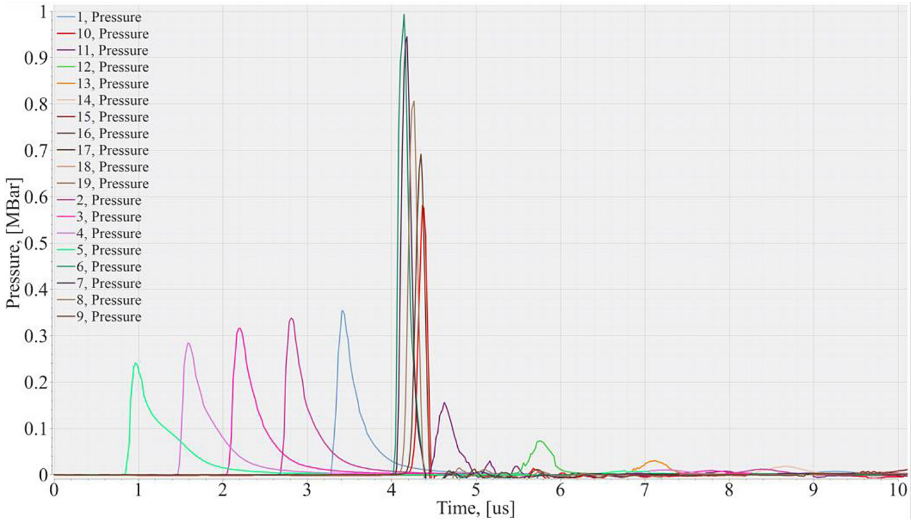

Figure 11. Tracer nodes pressure histories for 2.5 mm thick barrier and no detonation

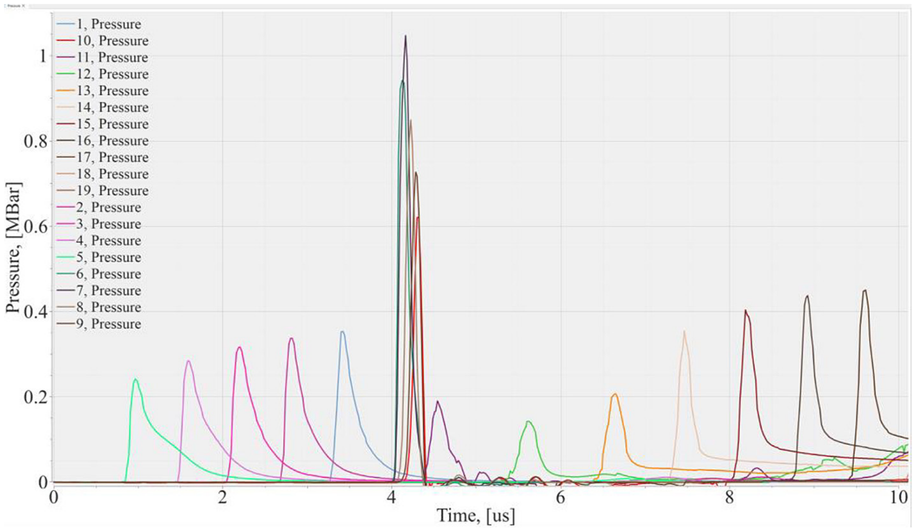

Figure 12. Tracer nodes pressure histories for 2.0 mm thick barrier and detonation

CONCLUSIONS

On the basis of the works presented in the article, the following conclusions can be drawn:

A numerical model of the phenomenon of detonation propagation from the donor to acceptor charges separated by a metal barrier was built. The model was verified against available data, and the high agreement between simulation and experimental results makes it possible to use the model to support experimental testing.

Two models of the igniter were examined. In the first model, the frontal part is flat, while in the second model, the front has a spherical cavity. For both models of the igniter, a series of computer simulations were performed for a steel barrier of different thicknesses. The results for both models differ for the same barrier thickness. The second solution more effectively ignite the donor charge through a barrier in (maximum barrier thickness for which the detonation was observed equaled 2.0 mm). The advantage of a fuse with a spherical cavity lies in the concentration of explosive energy near the axis of the fuse, similar to cumulative charges and EFP projectiles. The results of analyses of TNT charge initiation through the steel barrier indicate little significance of the material used for the ERG electric igniter casing (aluminum and copper casings were used).

Experimental tests have shown that the minimum thickness of a steel plate with a hardness of 63 HRC that effectively protects the TNT charge from being detonated by an ERG-type detonator is 3.5 mm. It is proposed to conduct such tests, for explosives other than TNT. The method used for the study, which uses ERG-type electric detonators as standard stimuli to produce shock loads, can be used to test the sensitivity to shock stimulation of other high explosives. Explosives with low sensitivity to shock loading would require a large-scale "gap test" method.

REFERENCES

1. Overton I., Davies R., and Tumchewics L. Improvised Explosive Devices: Past, Present And Future, Action on armed violence AOAV, 405 Mile End Road, London E3 4PB, https://aoav.org.uk/wp-content/uploads/2020/10/IEDs-past-present-and-future.pdf
2. https://d2071andvip0wj. cloudfront. net/exploiting-disorder-al-qaeda-and-the-islamic-state. pdf. J. 2020 International Crisis Group, Exploiting Disorder: Al- Qaeda and the Islamic State, Mar. 2016.
3. Ramasamy A., Masouros S. D., Newell N., et al. In-vehicle extremity injuries from improvised explosive devices: Current and future foci, in Philosophical Transactions of the Royal Society B: Biological Sciences, 2011. https://doi.org/10.1098/rstb.2010.0219
4. https://en.wikipedia.org/wiki/Improvised_explosive_device - web page containing general description of the improvised explosive device idea and principles. Access - December 2023.
5. Krysiński B., Borkowski J. Patent No. PL 222935, Method of blocking direct access to the main charge of an explosive material elaborated in the shell, in particular a projectile, by means of a special protective barrier. (in polish: Sposób zablokowania bezpośredniego dostępu do zasadniczego ładunku materiału wybuchowego zaelaborowanego w skorupie środka bojowego, zwłaszcza pocisku za pomocą specjalnego przegrody zabezpieczającej), 14.03.2013, Polish Patent Office.
6. Hudson L. C. and Bernecker R. R. Numerical calibration of donor systems for some GAP tests, Propellants, Explosives, Pyrotechnics, 1995, 20(6), https://doi.org/10.1002/prep.19950200609
7. Bourne N. K., Milne A., and Biers R. A. Measurement of the pressure pulse from a detonating explosive, J Phys D Appl Phys, 2005, 38(12), https://doi.org/10.1088/0022-3727/38/12/019
8. Qiang H. F., Liu Y. X., Wang D. D., Wang X. R., Geng B., and Wang G. Numerical simulation study of composite solid propellant small scale gap test, AIP Adv, 2021, 11(1), https://doi.org/10.1063/5.0039853
9. Yan D., Bian D., Zhao J., and Niu S. Study of the electrical characteristics, shock-wave pressure characteristics, and attenuation law based on pulse discharge in water, Shock and Vibration, 2016, 2016, https://doi.org/10.1155/2016/6412309
10. Qing Xue Z., Li S., Liang Xin C., Ping Shi L., and Bin Wu H. Modeling of the whole process of shock wave overpressure of free-field air explosion, Defence Technology, 2019, 15(5), https://doi.org/10.1016/j.dt.2019.04.014
11. Karinski Y. S., Feldgun V. R., and Yankelevsky D. Z. Effect of soil locking on the cylindrical shock wave's peak pressure attenuation, J Eng Mech, 2009, 135(10), https://doi.org/10.1061/(asce)em.1943-7889.0000042
12. Bai Z., Duan Z., Wen L., Zhang Z., Ou Z., and Huang F. Embedded manganin gauge measurements and modelling of shock initiation in HMX-Based pbx explosives with different particle sizes and porosities, Propellants, Explosives, Pyrotechnics, 2020, 45(6), https://doi.org/10.1002/prep.201900376
13. Bai Z., Duan Z., Wen L., Zhang Z., Ou Z., and Huang F. Shock initiation of multi-component insensitive PBX explosives: Experiments and MC-DZK mesoscopic reaction rate model, J Hazard Mater, 2019, 369, https://doi.org/10.1016/j.jhazmat.2019.02.028
14. Ferdowsi M., Yazdani F., Omidkhah M. R., and Keshavarz M. H. Reliable prediction of shock sensitivity of energetic compounds based on small-scale gap test through their electric spark sensitivity, Z Anorg Allg Chem, 2018, 644(16), https://doi.org/10.1002/zaac.201800190
15. Lu J. P., Lochert I. J., Daniel M. A., and Franson M. D. Shock sensitivity studies for PBXN-109, Propellants, Explosives, Pyrotechnics, 2016, 41(3), https://doi.org/10.1002/prep.201500336
16. Nandlall D. Determination of a measure of sensitivity to shock detonate an explosive as a function of its shock parameters, Propellants, Explosives, Pyrotechnics, 2019, 44(11), https://doi.org/10.1002/prep.201800383
17. Kubota S., Ogata Y., Wada Y., et al. Observation of shock initiation process in gap test, in AIP Conference Proceedings, 2006. https://doi.org/10.1063/1.2263511
18. Price D. Gap Tests And How They Grow, in Minutes of the Explosives Safety Seminar (22nd), I, Anaheim, California: Naval Surface Weapons Center, Aug. 1986.
19. Kubota S., Liu Z., Otsuki M., Nakayama Y., Ogata Y., and Yoshida M. A numerical study of sympathetic detonation in gap test, in Materials Science Forum, 2004. https://doi.org/10.4028/www.scientific.net/msf.465-466.163
20. Kubota S., Liu Z., Saburi T., Ogata Y., and & Yoshida M. Simulation of sympathetic detonation by a CIP Eulerian code, 2005, Accessed: Jan. 11, 2024.

[Online]. Available: www.witpress.com,
21. Keshavarz M. H., Motamedoshariati H., Pouretedal H. R., Tehrani M. K., and Semnani A. Prediction of shock sensitivity of explosives based on small-scale gap test, J Hazard Mater, 2007, 145(1–2), https://doi.org/10.1016/j.jhazmat.2006.10.091
22. Maček A. Sensitivity of explosives, Chem Rev, 1962, 62(1), 41–63, https://doi.org/10.1021/CR60215A003 /ASSET/CR60215A003.FP.PNG_V03
23. Davies P. A. Accidental initiation of condensed phase explosives during road and rail transport, J Hazard Mater, 1994, 38(1), https://doi.org/10.1016/0304-3894(93)00003-L
24. Kim B., Park J., and Yoh J. J. Analysis on shock attenuation in gap test configuration for characterizing energetic materials, J Appl Phys, 2016, 119(14), https://doi.org/10.1063/1.4945777
25. Xia M., Wang J., and Jiang N. Critical shock wave initiation pressure of typical energetic materials, Sci. Technol. Energ. Mater., 2022, 83(2).
26. Matsumura T., Ishikawa K., Homae T., Wakabayashi K., and Nakayama Y. Card gap tests of plastic high explosive by using mortar, light weight concrete and sand as gap materials, Science and Technology of Energetic Materials, 2010, 71(5–6).
27. Tan B., Long X., Peng R., Li H., Jin B., and Chu S. On the shock sensitivity of explosive compounds with small-scale gap test, Journal of Physical Chemistry A, 2011, 115(38), https://doi.org/10.1021/jp204814f
28. Schwer L. E. Impact and Detonation of COMP-B An Example using the LS-DYNA ® EOS: Ignition and Growth of Reaction in High Explosives, 12 th International LS-DYNA ® Users Conference, 2012.
29. Urtiew P. A., Vandersall K. S., Tarver C. M., Garcia F., and Forbes J. W. Shock initiation of composition b and C-4 explosives: Experiments and modeling, Russian Journal of Physical Chemistry B, 2008, 2(2), https://doi.org/10.1134/S1990793108020036
30. Urtiew P. A., Vandersall K. S., Tarver C. M., Garcia F., and Forbes J. W. Shock initiation experiments and modeling of composition b and c-4, in Proceedings of the 13th International Detonation Symposium, IDS 2006, 2006.
31. Balagansky I. A. and Stepanov A. A. Numerical simulation of Composition B high explosive charge desensitization in gap test assembly after loading by precursor wave, Shock Waves, 2016, 26(2), https://doi.org/10.1007/s00193-015-0584-1
32. Żochowski P. and Warchoł R. Experimental and numerical study on the influence of shaped charge liner cavity filing on jet penetration characteristics in steel targets, Defence Technology, 2023, 23, https://doi.org/10.1016/j.dt.2022.09.007
33. https://www.impetus.no/ - web page containing general description of the Impetus AFEA numerical analysis software used and the computational methods available. Access - December 2023.
34. https://www.abstrao.com/en/gamma-sph-add-on - web page containing general description of the Gamma-SPH particle based (meshless) computational method used in the article. Access - December 2023.
35. https://www.impetus.no/support/manual/ - web page containing list of available commands in Impetus AFEA software. Access - December 2023.
36. ANSYS Help, Release 16.0, 2015 – a manual built into the ANSYS software containing a description of the commands and material models available for calculations. Access - December 2023.
37. Johnson G. R. and Cook W. H. A constitutive model and data for metals subjected to large strains, high strain rates and high temperatures. The 7th International Symposium on Ballistics, in Proceedings of the 7th International Symposium on Ballistics, 1983.
38. LS-DYNA® Keyword User's Manual; LS-DYNA R12. II, Materials Models. (r:13191), Sep. 2020. a manual for the Ls-Dyna software containing a description of the material models available for calculations. Access - December 2023.